ANALYSIS OF RADIATION CHARACTERISTICS OF AN OPEN CIRCULAR WAVEGUIDE ASYMMETRICALLY COVERED BY A DIELECTRIC LAYERED HEMI-SPHERICAL RADOME

M. S. Leong, L. W. Li [†], X. Ma, P. S. Kooi, and T. S. Yeo

Department of Electrical and Computer Engineering
National University of Singapore
10 Kent Ridge Crescent, Singapore 119260

Abstract—In this paper, the radiation characteristics of an open circular waveguide asymmetrically covered by a layered dielectric hemi-spherical radome are analyzed. On the waveguide opening, the dominant TE_{11} wave of the circular waveguide is assumed. The technique of dyadic Green's function is applied to obtain the radiated electromagnetic fields due the circular aperture. Huygens' equivalence principle and the image theory are utilized to simplify the problem. The translational addition theorems of spherical vector wave functions are also employed to make the mathematical representation of the radiated fields compact. Both the exact formulation in the near (radiating-field) zone and the approximate expressions in the far (Fraunhofer) zone of the radiated fields are obtained. Numerical computations are implemented to show the effects of the off-centered source feed asymmetrically covered by the hemi-spherical dielectric radome.

1 Introduction

2 Statement of the Problem

3 Formulation of EM Fields

4 Numerical Results

[†] High Performance Computation for Engineered Systems, Singapore-MIT Alliance, 10 Kent Ridge Crescent, Singapore 119260

5   Conclusion

Acknowledgment

References

1. INTRODUCTION

For protecting the antenna radiation system from the environmental
effects such as rainfall, dust, tiny sand particles, and snow, a
dielectric radome has been frequently used and has been an important
component in antenna systems, as indicated in the excellent references
by Walton [1] and by Crone *et al.* [2].   A dielectric radome takes
different configurations in shape, of which the most common ones
are the planar, cylindrical, spherical, and oblate spheroidal for many
civil applications [3–8]; and conic, paraboloidal, tangent ogival, prolate
spheroidal, and superspheroidal for many military applications [1, 2, 9].
Due to the presence of a radome, the performance of an antenna system
can be affected.   It is known that the far-field pattern distortions,
transmission loss, low angular aberrations (the angular difference
between a target's actual and radar-indicated position) and small
sidelobe degradations, co-polar and cross-polarizations, and *boresight
error* (BSE) are the most common effects of the protective radome.

The effects of radome have been previously investigated using
traditional approaches such as ray tracing technique, with which
analysis of the antenna radomes fails at lower frequencies.   Various
methods were developed over the past few decades.   The methods
available elsewhere in the literature for analyzing the dielectric radome
are: (i) the *R*ay *T*racing *T*echnique (RTT) [1, 2, 10] which is the
most popular one, (ii) the (Single) Plane Wave Spectrum-Surface
Integral Technique [11, 12], (iii) the *P*hysical *O*ptics (PO) method
and *D*ielectric *P*hysical *O*ptics (DPO) technique [13], (vi) the *M*oment
*M*ethod (MM) or *M*ethod *o*f *M*oment (MoM) [13], (v) the *F*inite
*E*lement *M*ethod (FEM) [14, 15], (iv) a hybrid method that combines
the Green's function approach that accounts for the radome and
the *M*ethod *o*f *R*egularization (MoR) for solving the scattering from
reflector accurately was proposed [16].

Since the actual source in radome engineering is sometimes located
somewhat off-center of a hemi-spherical shell radome as a result
of positioning tolerance, this paper aims at analyzing the radiation
characteristics of a circular aperture antenna in the presence of a
hemi-spherically multilayered dielectric radome.   It is assumed that
such an aperture fed by a circular waveguide is *asymmetrically* covered
by a hemi-spherical radome.   Therefore, the translational addition

theorems for spherical vector wave functions [17–19], together with the dyadic Green's function technique, are employed in the analysis of the radiated EM fields so as to gain an insight into the distortion. Huygens' equivalence principle and image theory are also utilized to simplify the problem. In this paper, numerical calculations are also carried out with *Mathematica*, a software of Wolfram Research, Inc., to show the effects of the off-centered source and the dielectric radome. It is evident that when a single hemi-spherical dielectric resonator is placed over the ground plane, the analysis due to a wire antenna could be easily carried out [20]. However, when an aperture placed off-center inside a dielectric radome, analysis becomes quite involved and hence requires intensive numerical computations.
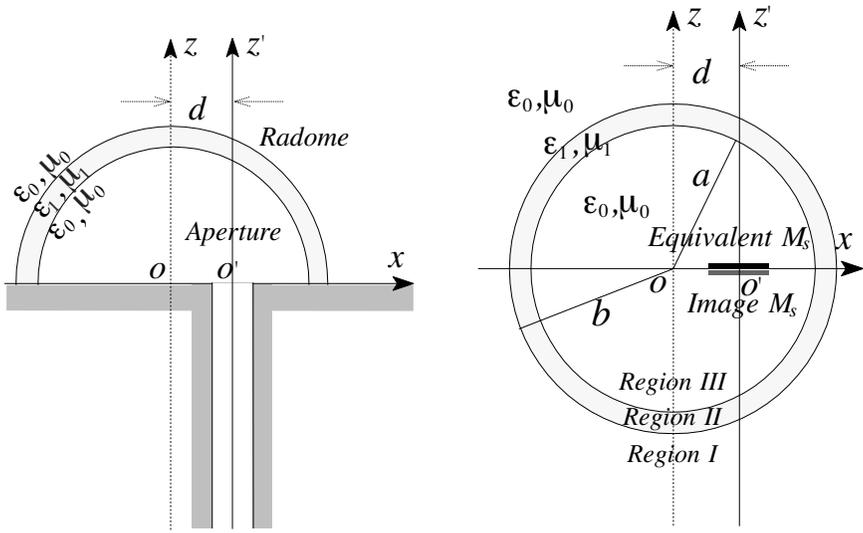
2. STATEMENT OF THE PROBLEM

The configuration of the problem to be considered is shown in Fig. 1(a). As can be seen from the geometry, a spherical layered radome, either single- or multi-layered, covers a circular aperture. The aperture source is an open circular waveguide excited by the dominant TE_{11} mode off-center placed inside the dielectric spherical shell radome.

The center of the aperture is located at $(r_0, \pi/2, \phi_0)$ generally, as shown in Fig. 1(a). To simplify the mathematical derivation, $\phi_0 = 0$ is assumed since the $\hat{x}$-axis can be arbitrarily chosen. Due to the presence of the conducting plane, the original radiation problem is equivalent to the radiation from the real source and its image source by applying Huygens' principle and image theory, as shown in Fig. 1(b). The center of the image is therefore located at $(r_0, \pi/2, \phi_0)$ inside the radome. The total field from the antenna radiation due to the off-center source is the addition of the contributions from both real source and image source. Finally, to simplify the problem we will further consider the radiated far field due to the real source and its image.

3. FORMULATION OF EM FIELDS

Due to the presence of the layered radome, the free space is divided into three regions labelled as I, II, and III. The radiated electromagnetic fields, $\boldsymbol{E}_f$ and $\boldsymbol{H}_f$ in the f-th region ($f = 1, 2$, and 3) due to the magnetic current distribution $\boldsymbol{M}_s$ located in the 3-th region ($s = 3$ for the inner-most region), are expressed in terms of the dyadic Green's function as follows:

$$\boldsymbol{E}_f(\boldsymbol{r}) = -\iiint_V \boldsymbol{\nabla} \times \overline{\boldsymbol{G}}_m^{(fs)}(\boldsymbol{r}, \boldsymbol{r}') \cdot \boldsymbol{M}_s(\boldsymbol{r}') dV', \qquad \text{(1a)}$$

(a) Configuration

(b) Huygens' equivalence of the problem
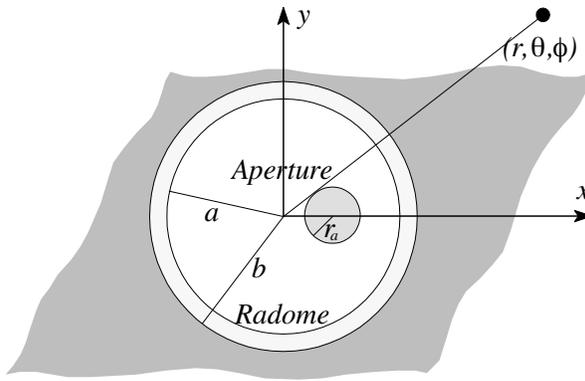
(c) Top view of the off-center feed problem

Figure 1. Radiation of an off-center circular waveguide feed covered by a spherical shell radome.

$$\boldsymbol{H}_f(\boldsymbol{r}) = i\omega\varepsilon_f \iiint_V \overline{\boldsymbol{G}}_m^{(fs)}(\boldsymbol{r}, \boldsymbol{r}') \cdot \boldsymbol{M}_s(\boldsymbol{r}')dV', \qquad (1b)$$

where the prime denotes the coordinates (r', θ', ϕ') of the current source $\boldsymbol{M}_s$, V identifies the volume occupied by the source in region III, $\overline{\boldsymbol{G}}_m^{(fs)}(\boldsymbol{r}, \boldsymbol{r}')$ denotes the magnetic type of dyadic Green's function, ε_f, μ_f and σ_f identify the permittivity, permeability and conductivity of the medium, respectively, and the propagation constant in the f-th region of the multilayered medium is designated as $k_f = \omega\sqrt{\mu_f\varepsilon_f\left(1 + \frac{i\sigma_f}{\omega\varepsilon_f}\right)}$. Since the inner-most and outer-most regions are filled with air, so we have $\varepsilon_1 = \varepsilon_3 = \varepsilon_0$, $\mu_1 = \mu_3 = \mu_0$ and $\sigma_1 = \sigma_3 = 0$.

The magnetic source $\boldsymbol{M}_s(\boldsymbol{r}')$ due to the assumed TE$_{11}$ dominant mode excitation in the original unprimed coordinate system is complicated. In the primed coordinate system, however, it is expressed as follows [21]:

$$\boldsymbol{M}_s(\boldsymbol{r}'') = 2\left[E_\phi\widehat{\boldsymbol{\rho}} - E_\rho\widehat{\boldsymbol{\phi}}\right] = 2E_0\left[\widehat{\boldsymbol{r}}\frac{dJ_1(\chi_{11}r''/r_a)}{dr''}\cos\phi''\right.$$
$$\left. - \widehat{\boldsymbol{\phi}}\frac{J_1(\chi_{11}r''/r_a)}{r''}\sin\phi''\right]\frac{\delta\left(\theta'' - \frac{\pi}{2}\right)}{r''}, \qquad (2)$$

where $\chi_{11}(= 1.84118)$ is the first root of the derivative of the first order cylindrical Bessel function, i.e. $J_1'(x)$. It is tested in [22] that when the radome size is much larger than the wavelength used, the feed-back effects on the source distribution due to the radome multiple reflections can be neglected.

The generalized dyadic Green's functions in terms of spherical vector wave functions $\boldsymbol{M}_{emn}$ and $\boldsymbol{N}_{emn}$ for the radially multilayered media have been constructed and their scattering (in fact transmission) coefficients have been derived by Li et al. [23]. For the sake of convenient application of the translational addition theorems, this paper uses the spherical vector wave functions $\boldsymbol{M}_{mn}$ and $\boldsymbol{N}_{mn}$. Careful check shows that, except for the factor $(2 - \delta_{m0})$ which is changed to unity and the duality must be applied, there is no other change in the dyadic Green's functions (including their coefficients) given by [23].

By making use of the magnetic dyadic Green's function $\overline{\boldsymbol{G}}_m^{(13)}$ in [23], the electric field in the first region outside the radome can be expressed by

$$\boldsymbol{E}_1 = -\iiint_V \boldsymbol{\nabla} \times \overline{\boldsymbol{G}}_m^{(13)} \cdot \boldsymbol{M}_s dV'$$
$$= -\frac{ik_0^2}{8\pi}\sum_{n=1}^{\infty}\sum_{m=0}^{n}\frac{(2n+1)}{n(n+1)}\frac{(n-m)!}{(n+m)!}$$

$$\cdot \left[\mathcal{A}_{13}^{TM} \boldsymbol{N}_{mn}^{(1)}(k_0) \iiint_V \boldsymbol{M}'_{mn}(k_0) \cdot \boldsymbol{M}_s dV' \right.$$

$$\left. + \mathcal{A}_{13}^{TE} \boldsymbol{M}_{mn}^{(1)}(k_0) \iiint_V \boldsymbol{N}'_{mn}(k_0) \cdot \boldsymbol{M}_s dV' \right], \qquad (3)$$

where the scattering coefficients of the magnetic dyadic Green's functions, $\mathcal{A}_{13}^{TE}$ and $\mathcal{A}_{13}^{TM}$ for TE and TM modes, are given by [23], the spherical vector wave functions in explicit form are supplied as follows for readers' convenience:

$$\boldsymbol{M}_{mn}(k) = \frac{im}{\sin\theta} z_n(kr) P_n^m(\cos\theta) e^{im\phi} \widehat{\boldsymbol{\theta}}$$
$$- z_n(kr) \frac{dP_n^m(\cos\theta)}{d\theta} e^{im\phi} \widehat{\boldsymbol{\phi}}, \qquad (4a)$$

$$\boldsymbol{N}_{mn}(k) = \frac{n(n+1)}{kr} z_n(kr) P_n^m(\cos\theta) e^{im\phi} \widehat{\boldsymbol{r}}$$
$$+ \frac{1}{kr} \frac{d[rz_n(kr)]}{dr} \frac{dP_n^m(\cos\theta)}{d\theta} e^{im\phi} \widehat{\boldsymbol{\theta}}$$
$$+ \frac{im}{\sin\theta} \frac{d[rz_n(kr)]}{krdr} P_n^m(\cos\theta) e^{im\phi} \widehat{\boldsymbol{\phi}}, \qquad (4b)$$

and the magnetic current distribution $\boldsymbol{M}_s$ in the present coordinate system cannot be simply expressed and also the triple integration ranges are not independent.

To make the problem easier, the vector translational addition theorems provide a straightforward way. The translational addition theorems to be applied for spherical vector wave functions [17–19] are given under the coordinate translation shown in Fig. 2 as follows:

$$\boldsymbol{M}'_{mn} = \sum_{r=0}^{\infty} \sum_{\mu=-\nu}^{\nu} \left(A_{\mu\nu}^{mn} \boldsymbol{M}''_{\mu\nu} + B_{\mu\nu}^{mn} \boldsymbol{N}''_{\mu\nu} \right), \qquad (5a)$$

$$\boldsymbol{N}'_{mn} = \sum_{r=0}^{\infty} \sum_{\mu=-\nu}^{\nu} \left(A_{\mu\nu}^{mn} \boldsymbol{N}''_{\mu\nu} + B_{\mu\nu}^{mn} \boldsymbol{M}''_{\mu\nu} \right), \qquad (5b)$$

where $\boldsymbol{M}''_{\mu\nu}$ and $\boldsymbol{N}''_{\mu\nu}$ are spherical vector wave functions in the o'' coordinate system, and the coefficients $A_{\mu\nu}^{mn}$ and $B_{\mu\nu}^{mn}$ will be given subsequently in (11).

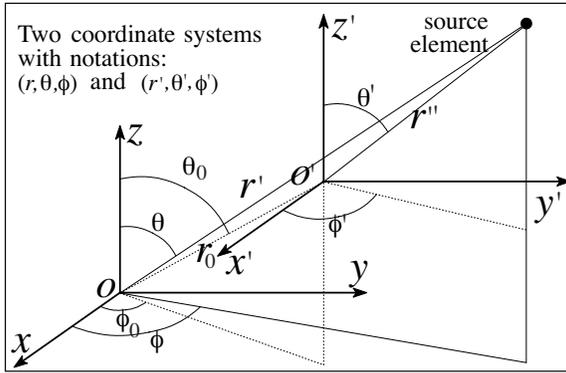Substitutions of Eq. (5) into Eq. (3) leads the electric field in

Figure 2. Spherical coordinate translation.

Eq. (3) becoming:

$$\boldsymbol{E}_1 = -\frac{ik_0^2}{4\pi}\sum_{n=1}^{\infty}\sum_{m=0}^{n}\frac{(2n+1)}{n(n+1)}\frac{(n-m)!}{(n+m)!}$$

$$\cdot\left[\mathcal{A}_{13}^{TM}\boldsymbol{N}_{mn}^{(1)}(k_0)\sum_{\nu=0}^{\infty}\sum_{\mu=-\nu}^{\nu}\iiint_{V}\left(A_{\mu\nu}^{mn}\boldsymbol{M}_{\mu\nu}''+B_{\mu\nu}^{mn}\boldsymbol{N}_{\mu\nu}''\right)\cdot\boldsymbol{M}_s dV'\right.$$

$$\left.+\mathcal{A}_{13}^{TE}\boldsymbol{M}_{mn}^{(1)}(k_0)\sum_{\nu=0}^{\infty}\sum_{\mu=-\nu}^{\nu}\iiint_{V}\left(A_{\mu\nu}^{mn}\boldsymbol{N}_{\mu\nu}''+B_{\mu\nu}^{mn}\boldsymbol{M}_{\mu\nu}''\right)\cdot\boldsymbol{M}_s dV'\right]$$

$$= -\frac{ik_0^2 E_0}{4\pi}\sum_{n=1}^{\infty}\sum_{m=0}^{n}\frac{(2n+1)}{n(n+1)}\frac{(n-m)!}{(n+m)!}$$

$$\cdot\left[\mathcal{A}_{13}^{TM}\boldsymbol{N}_{mn}^{(1)}\sum_{\nu=1}^{\infty}\left(A_{\mu\nu}^{mn}\Phi_\nu + B_{\mu\nu}^{mn}\Psi_\nu\right)\right.$$

$$\left.+\mathcal{A}_{13}^{TE}\boldsymbol{M}_{mn}^{(1)}\sum_{\nu=1}^{\infty}\left(A_{1\nu}^{mn}\Psi_\nu + B_{1\nu}^{mn}\Phi_\nu\right)\right], \qquad (6)$$

where only the term for $\mu = 1$ exists in the summation of μ because the corresponding mode has non-zero integration with $\hat{\boldsymbol{y}}$ polarized TE_{11} source, and Φ_ν and Ψ_ν are expressed as:

$$\Phi_\nu = \frac{i}{2E_0}\iiint_{V}\boldsymbol{M}_{o1\nu}\cdot\boldsymbol{M}_s dV'$$

$$= i\pi\left.\frac{dP_\nu^1(\cos\theta)}{d\theta}\right|_{\theta=90°}\int_0^{r_0}j_\nu(k_0 r')J_1(k_c r')dr', \qquad (7a)$$

$$\Psi_\nu = \frac{1}{2E_0}\iiint_V \boldsymbol{N}_{e1\nu} \cdot \boldsymbol{M}_s dV'$$

$$= \frac{\pi}{k_0}P_\nu^1(0)\left[\nu(\nu+1)\int_0^{r_0}\frac{d[J_1(k_cr')]}{dr'}j_\nu(k_0r')dr'\right.$$

$$\left. + \int_0^{r_0}J_1(k_cr')\frac{d[r'j_\nu(k_0r')]}{r'dr'}dr'\right]. \tag{7b}$$

Furthermore, the explicit form of Eq. (6) becomes:

$$E_r = \frac{-ik_0^2E_0}{4\pi}\sum_{n=1}^\infty\sum_{m=0}^\infty\frac{(2n+1)}{n(n+1)}\frac{(n-m)!}{(n+m)!}e^{im\phi}$$

$$\cdot\frac{n(n+1)}{kr}A_{13}^{TM}h_n^{(1)}(k_0r)P_n^m(\cos\theta)$$

$$\cdot\sum_{\nu=1}^\infty(A_{1\nu}^{mn}\Phi_\nu + B_{1\nu}^{mn}\Psi_\nu), \tag{8a}$$

$$E_\theta = \frac{-ik_0^2E_0}{4\pi}\sum_{n=1}^\infty\sum_{m=0}^\infty\frac{(2n+1)}{n(n+1)}\frac{(n-m)!}{(n+m)!}e^{im\phi}$$

$$\left[A_{13}^{TM}\frac{d\left[rh_n^{(1)}(k_0r)\right]}{k_0rdr}\frac{dP_n^m(\cos\theta)}{d\theta}\right.$$

$$\cdot\sum_{\nu=1}^\infty(A_{1\nu}^{mn}\Phi_\nu + B_{1\nu}^{mn}\Psi_\nu) + A_{13}^{TE}h_n^{(1)}(k_0r)$$

$$\left.\cdot\frac{imP_n^m(\cos\theta)}{\sin\theta}\sum_{\nu=1}^\infty(A_{1\nu}^{mn}\Psi_\nu + B_{1\nu}^{mn}\Phi_\nu)\right], \tag{8b}$$

$$E_\phi = \frac{-ik_0^2E_0}{4\pi}\sum_{n=1}^\infty\sum_{m=0}^\infty\frac{(2n+1)}{n(n+1)}\frac{(n-m)!}{(n+m)!}e^{im\phi}$$

$$\cdot\left[A_{13}^{TM}\frac{d\left[rh_n^{(1)}(k_0r)\right]}{k_0rdr}\frac{im}{\sin\theta}P_n^m(\cos\theta)\right.$$

$$\cdot\sum_{\nu=1}^\infty(A_{1\nu}^{mn}\Phi_\nu + B_{1\nu}^{mn}\Psi_\nu) - A_{13}^{TE}h_n^{(1)}(k_0r)$$

$$\left.\cdot\frac{dP_n^m(\cos\theta)}{d\theta}\sum_{\nu=1}^\infty(A_{1\nu}^{mn}\Psi_\nu + B_{1\nu}^{mn}\Phi_\nu)\right]. \tag{8c}$$

The Fraunhofer fields can be further obtained by making use of the far-zone approach. For the field region in the far-zone or under the

high-frequency approximation $kr \gg n^2$, the Hankel function and its derivative can be expressed [24] by:

$$h_n^{(1)}(kr) \simeq (-i)^{n+1}\frac{e^{ikr}}{kr}, \tag{9a}$$

$$\frac{d[rh_n^{(1)}(kr)]}{dr} \simeq (-i)^n e^{ikr}. \tag{9b}$$

So the electric fields in the far-zone can be approximated as follows:

$$E_r \simeq 0, \tag{10a}$$

$$
\begin{aligned}
E_\theta = {} & \frac{E_0 k_0 e^{ik_0 r}}{4\pi r} \sum_{n=1}^\infty \sum_{m=0}^\infty (-i)^{n+1}\frac{(2n+1)}{n(n+1)}\frac{(n-m)!}{(n+m)!}e^{im\phi} \\
& \cdot \left[A_{13}^{TM}\frac{dP_n^m(\cos\theta)}{d\theta}\sum_{\nu=1}^\infty (A_{1\nu}^{mn}\Phi_\nu + B_{1\nu}^{mn}\Psi_\nu) \right. \\
& \left. + A_{13}^{TE}m\frac{P_n^m(\cos\theta)}{\sin\theta}\sum_{\nu=1}^\infty (A_{1\nu}^{mn}\Psi_\nu + B_{1\nu}^{mn}\Phi_\nu) \right],
\end{aligned}
\tag{10b}
$$

$$
\begin{aligned}
E_\phi = {} & \frac{E_0 k_0 e^{ik_0 r}}{4\pi r} \sum_{n=1}^\infty \sum_{m=0}^\infty (-i)^{n}\frac{(2n+1)}{n(n+1)}\frac{(n-m)!}{(n+m)!}e^{im\phi} \\
& \cdot \left[A_{13}^{TM}m\frac{P_n^m(\cos\theta)}{\sin\theta}\sum_{\nu=1}^\infty (A_{1\nu}^{mn}\Phi_\nu + B_{1\nu}^{mn}\Psi_\nu) \right. \\
& \left. + A_{13}^{TE}\frac{dP_n^m(\cos\theta)}{d\theta}\sum_{\nu=1}^\infty (A_{1\nu}^{mn}\Psi_\nu + B_{1\nu}^{mn}\Phi_\nu) \right],
\end{aligned}
\tag{10c}
$$

where by considering $\phi_0 = 0$, the intermediates are given by

$$
\begin{aligned}
A_{\mu\nu}^{mn} = {} & (-1)^\mu \sum_p a(m,n\,|-\mu,\nu\,|\,p)a(n,\nu,p) \\
& \cdot j_p(kr_0)P_p^{m-1}(\cos\theta_0),
\end{aligned}
\tag{11a}
$$

$$
\begin{aligned}
B_{\mu\nu}^{mn} = {} & (-1)^{\mu+1} \sum_p a(m,n\,|-\mu,\nu\,|\,p,p-1) \\
& \cdot b(n,\nu,p)j_p(kr_0)P_p^{m-1}(\cos\theta_0);
\end{aligned}
\tag{11b}
$$

where

$$
\begin{aligned}
a(n,\nu,p) = {} & i^{\nu+p-n}\left[2\nu(\nu+1)(2\nu+1) + (\nu+1)\right. \\
& \cdot (n-\nu+p+1)(n+\nu-p) - \nu(\nu-n+p+1) \\
& \left. \cdot (n+\nu+p+2)\right]/\left[2\nu(\nu+1)\right],
\end{aligned}
\tag{12a}
$$

$$b(n, \nu, p) = i^{\nu+p-n} \left[(n + \nu + p + 1)(\nu - n + p)(n - \nu + p) \right.$$
$$\left. \cdot (n + \nu - p + 1) \right]^{1/2} (2\nu + 1) / \left[2\nu(\nu + 1) \right]; \qquad (12b)$$

and

$$a(m, n \,|\mu, \nu|\, p) = \left[\frac{(n + m)!(\nu + \mu)!(p - m - \mu)!}{(n - m)!(\nu - \mu)!(p + m + \mu)!} \right]^{1/2}$$
$$\cdot (-1)^{m+\mu}(2p + 1) \begin{bmatrix} n & \nu & p \\ 0 & 0 & 0 \end{bmatrix} \begin{bmatrix} n & \nu & p \\ m & \mu & -m - \mu \end{bmatrix},$$

$$(12c)$$

$$a(m, n \,|\mu, \nu|\, p, q) = \left[\frac{(n + m)!(\nu + \mu)!(p - m - \mu)!}{(n - m)!(\nu - \mu)!(p + m + \mu)!} \right]^{1/2}$$
$$\cdot (-1)^{m+\mu}(2p + 1) \begin{bmatrix} n & \nu & p \\ m & \mu & -m - \mu \end{bmatrix} \begin{bmatrix} n & \nu & q \\ 0 & 0 & 0 \end{bmatrix},$$

$$(12d)$$

where

$$\begin{bmatrix} j_1 & j_2 & j_3 \\ m_1 & m_2 & m_3 \end{bmatrix}$$

is the Wigner 3-j symbol satisfying the condition that $m_1+m_2+m_3 = 0$ and j_1, j_2, j_3 are triangular. Also the following definitions have been used in the integration:

$$k_1 = k_3 = k_0 = \omega\sqrt{\epsilon_0\mu_0}, \qquad (13a)$$
$$k_c = \chi_{11}/r_a = 1.84118/r_a. \qquad (13b)$$

In a similar fashion, the field radiated due to the image source can be expressed in the same form as in Eq. (10), except for $A_{\mu\nu}^{mn}$ substituted by $A_{\mu\nu}'^{mn}$ and $B_{\mu\nu}^{mn}$ by $B_{\mu\nu}'^{mn}$. So $A_{\mu\nu}'^{mn}$ and $B_{\mu\nu}'^{mn}$ are expressed as:

$$A_{\mu\nu}'^{mn} = (-1)^{\mu} \cdot \sum_p a(m, n \,|-\mu, \nu|\, p)a(n, \nu, p)$$
$$\cdot j_p(kr_0)P_p^{m-1}\left[\cos(\pi - \theta_0)\right], \qquad (14a)$$
$$B_{\mu\nu}'^{mn} = (-1)^{\mu+1} \sum_p a(m, n \,|-\mu, \nu|\, p, p - 1)b(n, \nu, p)$$
$$\cdot j_p(kr_0)P_p^{m-1}\left[\cos(\pi - \theta_0)\right]. \qquad (14b)$$

4. NUMERICAL RESULTS

To show the effects of the off-centered aperture source excited by the circular dominant TE_{11} mode and those of its covering radome above the conducting plane (as shown in Fig. 1(c) for the top view), numerical calculations have been carried out with the *Mathematica* software of Wolfram Research, Inc. and the results are shown subsequently.

4.1. Lateral Displacement of Source Location

Due to the multiple summations (in this case it is a fourfold summation) in the expressions of the far-zone electric field in Eq. (10), care must be exercised in checking the existing singularity and iteration convergence, in particular, when the index n is much larger than the argument x in the computation of the spherical Bessel functions $z_n(x)$. In our computer codes, convergence can be well achieved when N, M and ν are greater than 20, and P greater than 15. However, the numerical calculation is computationally slow due to the quadri-summation; therefore only the case of the off-centered feed on the ground plane is considered in the computation. A typical case where the aperture antenna is located at $(d, \pi/2, 0)$ is assumed and thus the image is also located at $(d, \pi/2, 0)$.

The normalized power pattern of the radome-free antenna flush-mounted on the ground plane given by Balanis [25] is chosen as a reference for comparisons. Throughout the computation, the frequency $f = 3$ GHz (for a wavelength of $\lambda_0 = 0.1$ m), and the dimension of the aperture $r_a = 1.5\lambda_0$ are used for convenient comparison with previous results.

In the numerical computation, various values of the Wigner 3-j symbol are provided by the *Mathematica* software. Also, the following relation is used for the associate Legendre functions of the negative index $-\mu$:

$$P_\nu^{-\mu}(x) = e^{-2i\nu\pi} \frac{\Gamma(\nu - \mu + 1)}{\Gamma(\nu + \mu + 1)} P_\nu^\mu(x). \tag{15}$$

Fig. 3 shows the normalized Fraunhofer power patterns in E- and H-planes against spherical polar angle θ for three cases: case (1) the Balanis' radome-free result for an aperture antenna flush-mounted on the ground plane [25]; case (2) the radome-free result for a horizontally off-centered aperture source located a distance $d = 0.5\lambda_0$ on the ground plane; case (3) the result for the same antenna in case (2) but in the presence of radome whose inner radius $a = 5\lambda_0$ and thickness $b - a = \lambda_e/2$.
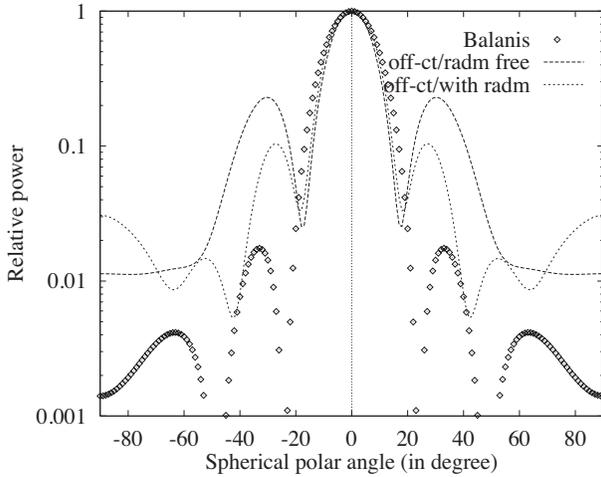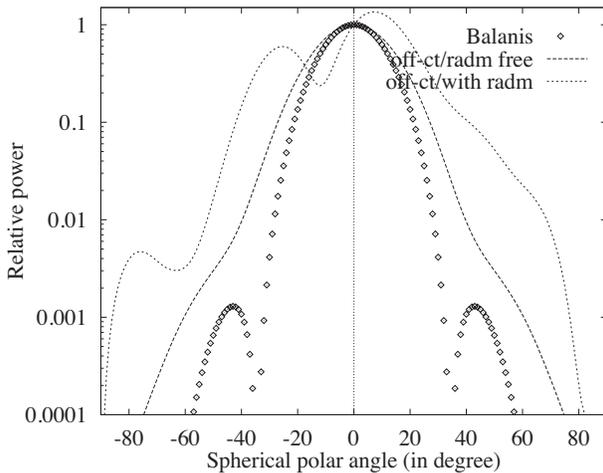
(a) *E*-plane power pattern

(b) *H*-plane power pattern

Figure 3. Normalized power patterns against the spherical polar angle (in degree) at 3 GHz. "*Balanis*" means the Balanis' result for a centered circular aperture in the absence of the radome. "*Off-ct rdm-free*" denotes the computed result for an off-centered aperture (located $(d, \pi/2, 0)$ where the displacement $d = 0.5\lambda_0$) in the absence of the radome. "*Off-ct with rdm*" represents the calculated result for the same off-centered aperture at the same location but in the presence of the radome with dimensions $a = 5\lambda_0$ and $b - a = \lambda_e/2$.

It can be seen that the normalized power pattern of the antenna in both the E- and H-planes changes dramatically when the aperture is shifted a horizontal distance (comparable to the wavelength) on the conducting plane. The main beam of the pattern is broadened in the E-plane and narrowed in the H-plane. Also, the first sidelobe level is increased, especially in the E-plane. Physically, this is reasonable because an opened waveguide in the absence of the ground plane has wider bandwidth. Due to the interaction of the shifted antenna on the conducting plane, the nulls of the pattern obviously also shift and the sidelobe levels change considerably. Thickness of a radome with medium size, such as $b - a = \lambda_e/6$, also considerably influences the antenna radiation further with increasing number of sidelobes and higher sidelobe levels. Since the original source is located on the x-axis, the pattern in the E-plane is symmetrical with respect to the spherical polar angle; but asymmetrical in the H-plane.

As illustration of the effects of the horizontal displacement, Fig. 4 depicts the far-zone power patterns in the E- and H-planes, respectively for the cases of horizontal displacements $d = 0.25\lambda_0$, $0.5\lambda_0$, $1.0\lambda_0$, and $2.0\lambda_0$. For the computed results shown in Fig. 4, it is assumed that $f = 3$ GHz, $a = 5\lambda_0$, and $b - a = \lambda_e/6$. It is seen from Fig. 4 that when the displacement distance d is electrically small (*e.g.*, $0.25\lambda_0$), the power pattern in the E-plane is not distorted much. However, the significant changes occur when the displacement is larger, especially when comparable with the wavelength. In both the E- and H-planes, dramatic variation of the power pattern is observed in Fig. 4 for the case where the aperture antenna is shifted to be very close to the antenna radome.

4.2. Cross-Polarization: Horizontally Displaced Source

The cross polarizations in the $\phi = 45°$ plane for an off-centred source excited by the dominant TE_{11} circular waveguide mode excluding (*"Balanis"* [25] and *"off-ct/radm free"*) and including effects of the radome (*"off-ct/with radm"*) are also computed and shown in Fig. 5. The parameters used in Fig. 5 are $r_a = 0.5\lambda_0$, $a = 3\lambda_0$, $b - a = \lambda_e/4$ and the aperture is off-centred at $(d, \pi/2, 0)$ where the displacement $d = \lambda_0$. We can see from the results that the cross polarization of an off-centred feed excited by the dominant TE_{11} mode increases considerably for most of the antenna pointing angles, compared to the case of centre-located feed. The presence of radome deteriorates the cross polarization further. The increase of the cross polarization is mainly due to the increased multiple interaction and interference among the feed, the radome, and the conducting ground plane.
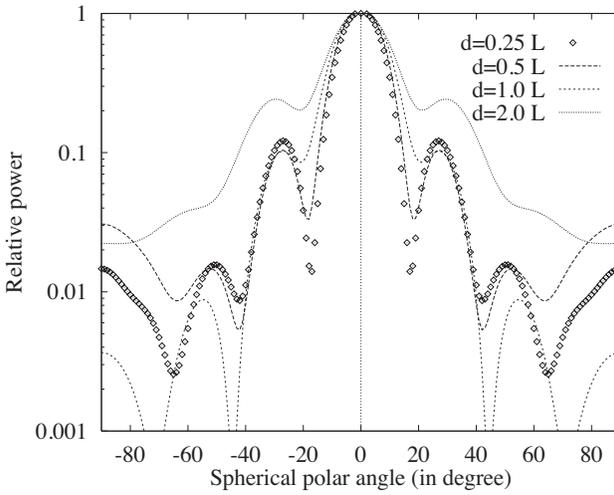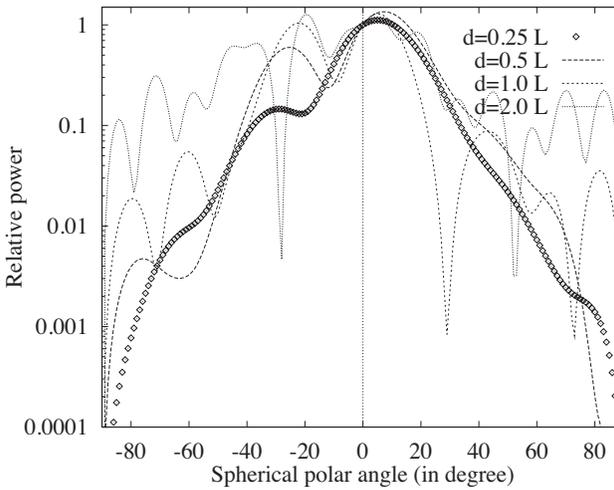
(a) *E*-plane power pattern

(b) *H*-plane power pattern

Figure 4. Normalized power patterns against the spherical polar angle (in degree) at 3 GHz. Inside this figure, L stands for λ_0 for simplicity. The horizontal displacement d away from the coordinate origin on the ground plane is assumed to be $0.25\lambda_0$, $0.5\lambda_0$, $1.0\lambda_0$, and $2.0\lambda_0$, respectively. The dimensions of the radome is $a = 5\lambda_0$ and $b - a = \lambda_e/6$.
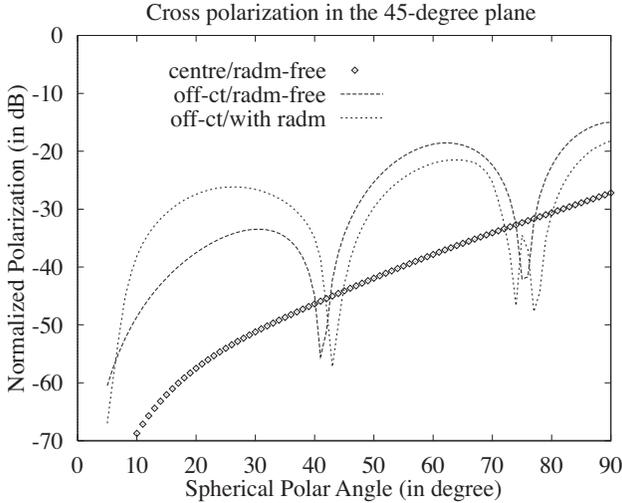
Cross polarization in the 45-degree plane

Figure 5. Cross polarization of radiated waves centrally and off-centrally excited by circular dominant TE_{11}-mode against spherical polar angle in the $\phi = 45^o$ plane in the absence and presence of the radome.

5. CONCLUSION

This paper presents a full-wave analysis of the radiation characteristics of an off-center located aperture excited by the circular waveguide dominant TE_{11} mode. The translational additional theorems for spherical vector wave functions [17–19] are applied in the analysis while dyadic Green's function technique, Huygens' equivalent principle and image theory are employed.

It has been found from the analysis that the interactions between the off-centered aperture source and the conducting plane become increasingly significant when d is larger than a quarter wavelength $\lambda_0/4$. These interactions result in considerable variations in main beamwidth, first sidelobe shape, position of nulls, and sidelobe levels of the power pattern. The presence of a dielectric radome with a thickness such as $\lambda_e/6$ rather than half a wavelength or its multiples influences the antenna radiation further. The combined effects of the off-centered feeding and the dielectric radome coverage degrade the antenna patterns even more.

ACKNOWLEDGMENT

REFERENCES

1. Walton Jr., J. D. (Ed.), *Radome Engineering Handbook: Design and Principles,* Marcel Dekker, Inc., New York, 1970.

2. Crone, G. A. E., A. W. Rudge, and G. N. Taylor, "Design and performance of airborne radomes: A review," *IEE Proc. Part F,* Vol. 128, 451–463, December 1981.

3. Chu, R.-S., "Analysis of an infinite phased array of dipole elements with RAM coating on ground plane and covered with dielectric radome," *IEEE Trans. Antennas Propagat.,* Vol. AP-39, No. 2, 164–176, 1991.

4. Shavit, R., A. P. Smolski, E. Michielssen, and R. Mittra, "Scattering analysis of high performance large sandwich radomes," *IEEE Trans. Antennas Propagat.,* Vol. AP-40, No. 2, 126–133, 1992.

5. Shavit, R., "Dielectric cover effect on rectangular microstrip antenna array," *IEEE Trans. Antennas Propagat.,* Vol. AP-42, No. 8, 1180–1184, 1994.

6. Bayard, J. P. R., "Analysis of infinite arrays of microstrip-fed dipoles printed on protruding dielectric substrates and covered with a dielectric radome," *IEEE Trans. Antennas Propagat.,* Vol. AP-42, No. 1, 82–89, 1994.

7. Vergnolle, C., T. Lemoine, and B. Dumont, "Material requirements for microwave antenna into aircraft skins," *Proceedings of Smart Structures and Materials 1993: Smart Materials,* 197–202, Albuquerque, NM, USA, February, 1993, Society of Photo-Optical Instrumentation Engineers, Bellingham, WA, USA.

8. Li, L.-W., P.-S. Kooi, M.-S. Leong, T.-S. Yeo, and X. Ma, "An analysis of a circular aperture antenna covered with a dielectric hemi-spherical shell radome over ground plane," *Digest of 1995 IEEE AP-S International Symposium and USNC/URSI Radio Science Meeting,* Vol. 3rd of 4, 1442–1445, Newport Beach, California, USA, June 18–23, 1995.

9. Overfelt, P. L., "Superspheroids: A new family of radome shapes," *IEEE Trans. Antennas Propagat.,* Vol. AP-43, No. 2, 215–220, 1995.

10. Deschamps, G. A., "Ray techniques in electromagnetics," *Proc. IEEE,* Vol. 60, No. 9, Sept. 1972.

11. Wu, D. C. F. and R. C. Rudduck, "Plane wave spectrum-surface integration technique for radome analysis", *IEEE Trans. Antennas Propagat.,* Vol. AP-22, 497–500, May 1974.

12. Paris, D. T., "Computer aided radome analysis," *IEEE Trans. Antennas Propagat.,* Vol. AP-18, 7–15, January 1970.

13. Hodges, R. E. and Y. Rahmat-Samii, "Evaluation of dielectric physical optics in electromagnetic scattering," *AP-S International Symposium (Digest) (IEEE Antennas and Propagation Society),* Vol. 3 (of 3), 1742–1745, Ann Arbor, MI, USA, June, 1993, IEEE Service Center, Piscataway, NJ, USA.

14. Gordon, R. K. and R. Mittra, "Finite element analysis of axisymmetric radomes," *IEEE Trans. Antennas Propagat.,* Vol. AP-41, No. 7, 975–981, 1993.

15. Ingalls, R. P., J. Antebi, J. A. Ball, R. Barvainis, J. F. Cannon, J. C. Carter, P. J. Charpentier, B. E. Corey, J. W. Crowley, K. A. Dudevoir, M. J. Gregory, F. W. Kan, S. M. Milner, A. E. E. Rogers, and J. E. Salah et al., "Upgrading the haystack radio telescope for operation at 115 Ghz," *Proc. IEEE,* Vol. 82, No. 5, 742–755, May 1994.

16. Svezhentsev, A. Y., A. I. Nosich, A. Altintas, and T. Oguzer, "Simulation of reflector antenna covered by a circular radome," *Proceedings of the 9th International Conference on Antennas and Propagation,* IEE, Stevenage, Engl., Part 1 (of 2), 532–535, Eindhoven, Neth, April, 1995.

17. Stein, S., "Addition theorems for spherical wave functions," *Quart. Appl. Math.,* Vol. 19, 15–24, 1961.

18. Cruzan, O. R., "Translational addition theorems for spherical vector wave functions," *Quart. Appl. Math.,* Vol. 20, 33–40, 1962.

19. Chew, W. C. and Y.-M. Wang, "Efficient ways to compute the vector addition theorem," *J. Electromagn. Waves Applic.,* Vol. 7, No. 5, 651–665, 1993.

20. Kishk, A. A., G. Zhou, and A. W. Glisson, "Analysis of dielectric-resonator antennas with emphasis on hemispherical structures," *IEEE Antennas and Propagation Magazine,* Vol. 36, No. 2, 20–31, April 1994.

21. Leong, M.-S., L.-W. Li, P.-S. Kooi, T.-S. Yeo, and X. Ma, "TE_{11}-

mode excitation of a circular aperture antenna covered by a layered dielectric hemi-spherical radome," *International Journal of Applied Electromagnetics & Mechanics,* Vol. 10, No. 3, 259–278, June 1999.

22. Li, L.-W., M.-S. Leong, L. Zhou, T.-S. Yeo, and P.-S. Kooi, "An improved analysis of antenna radiation from a circular aperture covered by a dielectric hemi-spherical radome shell," *IEE Proceedings on Microwave, Antennas and Propagation,* Vol. 147, No. 2, 144–150, April 1999.

23. Li, L.-W., P.-S. Kooi, M.-S. Leong, and T.-S. Yeo, "Electromagnetic dyadic Green's function in spherically multilayered media," *IEEE Trans. Microwave Theory Tech.,* Vol. 42, No. 12, Part A, 2302–2310, December 1994.

24. Stratton, J. A., *Electromagnetic Theory,* McGraw-Will, New York, 1941.

25. Balanis, C. A., *Antenna Theory: Analysis and Design,* 2nd edition, John Wiley & Sons, New York, 1997.